A Short Review of High-Temperature Wetting and Complexion Transitions with a Critical Assessment of Their Influence on Liquid Metal Embrittlement and Corrosion

Jian Luo[‡]

ABSTRACT

The basic concepts and new developments in the general areas of grain boundary segregation (adsorption), wetting, and complexion (interfacial phase-like) transitions are briefly reviewed. Subsequently, recent studies in several relevant areas are discussed. At the atomic level, the formation of bilayers in Ni-Bi and Cu-Bi have been observed and found to be the root cause for liquid metal embrittlement (LME). At the microstructural level, the presence of minor impurities or co-alloying elements can significantly enhance the intergranular penetration and liquid metal corrosion (LMC). Furthermore, triple-grain-line wetting by a liquid metal can occur at high temperatures, which may significantly affect corrosion resistance (for LMC), as well as LME. Somewhat surprisingly, Bi vapors can penetrate along the triple-grain lines in S-doped Ni specimens to form open channels, which can be considered as an unusual case of triple-line wetting by a vapor phase. A coherent theme of this review and critical assessment article is to explore the unrecognized, yet important, roles of high-temperature adsorption/segregation, wetting, and complexion transitions in LME and LMC.

KEY WORDS: adsorption, interfacial effects, intergranular corrosion, intergranular stress corrosion cracking, liquid metal corrosion, liquid metal embrittlement, stress corrosion cracking, thermodynamics

INTRODUCTION

When structural alloys are in contact with liquid metals (such as Bi and Pb), several modes of failures can occur. First, liquid metal corrosion (LMC) often takes place.[1-3] Second, intrinsically-ductile metals, such as Fe, Ni, Cu, and Al, can undergo catastrophic brittle intergranular fracture at unusually low stress levels; this phenomenon is called liquid metal embrittlement (LME).[4-11] Finally, the vapor phase of Bi and S can attack structural alloys and cause embrittlement and microstructural instability.[12-13]

This article briefly reviews the general theories and new developments in high-temperature grain boundary (GB) segregation (aka adsorption), wetting, and complexion (interfacial phase-like) transitions, with focuses on several recent new observations in Ni-Bi- and Cu-Bi-based systems (the solid primary phases are underlined) that are relevant to LME, LMC, and microstructural instability. These new discoveries include the formation of two-dimensional (2D) bilayer interfacial phases (also called complexions[14]) in Ni-Bi and Cu-Bi as the root cause for LME,[15-16] the significant influence minor impurities or co-alloying elements have on intergranular penetration and LMC,[17] the wetting of Ni triple-grain lines by Bi-enriched liquid,[16] and triple-line instability (wetting by a vapor phase) in (Bi + S) co-doped Ni system.[12] A coherent theme of this review and critical assessment article is to explore a unified interfacial thermodynamic framework to understand these new observations and their previously-unrecognized impacts on LME, LMC, and related materials degradation phenomena.

Submitted for publication: October 5, 2015. Revised and accepted: December 24, 2015. Preprint available online: December 24, 2015, http://dx.doi.org/10.5006/1925.

‡ Corresponding author. E-mail: jluo@alum.mit.edu. Department of NanoEngineering, Program of Materials Science and Engineering, University of California, San Diego, La Jolla, CA 92093-0448.

ISSN 0010-9312 (print), 1938-159X (online)

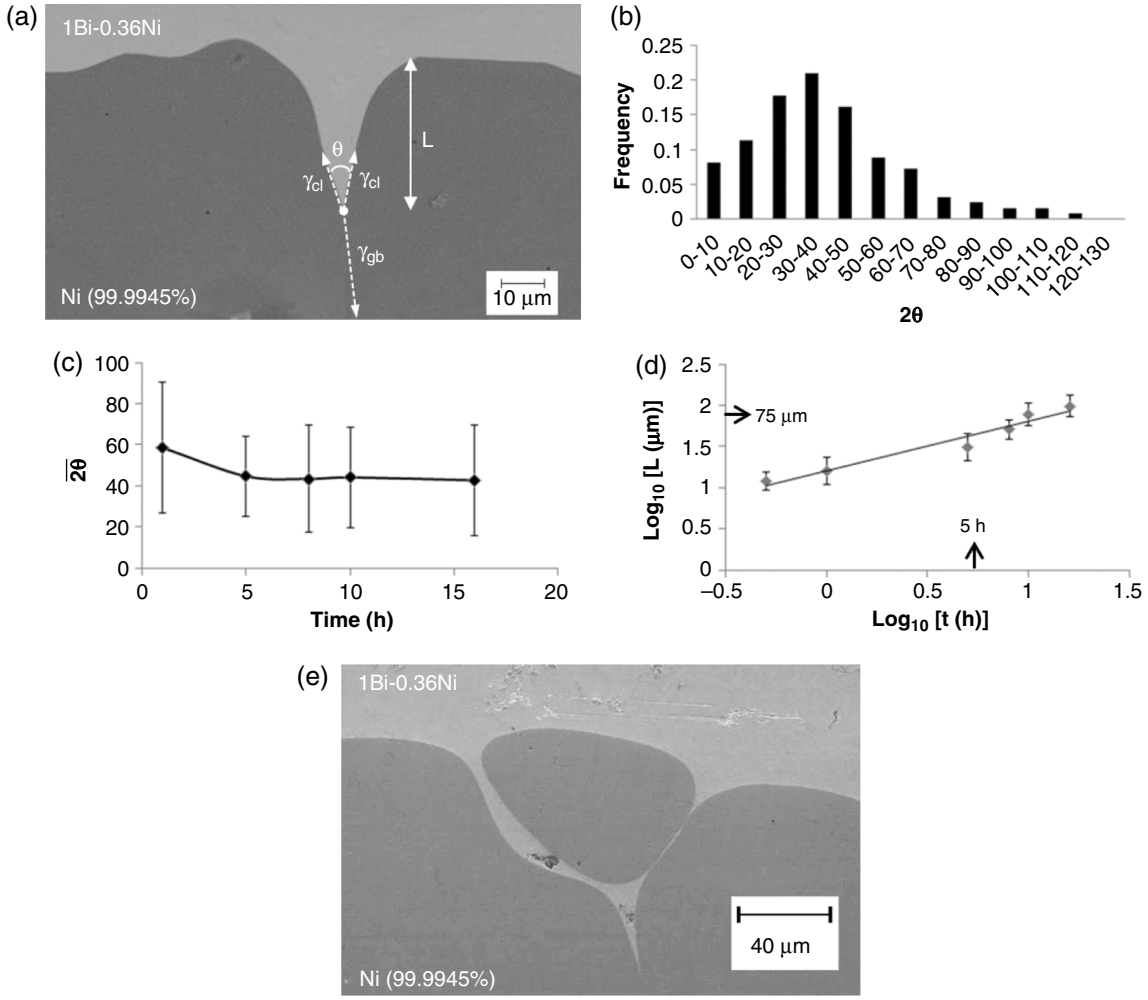

FIGURE 1. *Summary of the results of the intergranular penetration of the equilibrium Bi-Ni liquid in pure Ni at 700°C. (a) A cross-sectional scanning electron microscope (SEM) micrograph of a typical GB groove after annealing for 5 h. L is the penetration length and θ is the dihedral angle at the penetration tip. (b) The distribution of measured dihedral angles at different GBs in this specimen. (c) Measured average dihedral angle and (d) penetration length vs. annealing time. Note that the error bars in panel (c) represent the GB-to-GB variations of boundaries of different GB characters, as well as the effect of random 2D projections of 3D dihedral angles, which are significantly greater than the measurement errors in the average dihedral angles. (e) In a specimen that was annealed at 700°C for 16 h, the liquid penetration length exceeded the grain size. Reprinted (with minor revisions) from Asl and Luo,* Acta Mater. *60 (2012): p. 149-165,[17] with permission from Elsevier.*

It should be noted that most of the theories and experiments presented and discussed in this short review are about the behaviors of *average* general grain boundaries under equilibrium (or near-equilibrium) conditions. Practically, GB character and anisotropy in interfacial energies can result in significant GB-to-GB variations and other phenomena such as faceting. Kinetic limitations to equilibria, as well as the effects of applied stresses and radiation (that are important for applications in liquid metal cooled reactors), can often alter the LME and LMC behaviors. However, discussions of these advanced topics, where further studies have to be conducted to achieve comprehensive understandings (e.g., developing the theories of anisotropic and/or non-equilibrium complexion transitions), are beyond the scope of this short review.

GRAIN BOUNDARY WETTING AND LIQUID PENETRATION

Direct exposure of a solid metal to a liquid metal at a high temperature will result in the formation of grooves and the liquid penetration along the GBs of the solid metal. If a local equilibrium is achieved, the dihedral angle (θ) at the triple line (Figure 1[a]) is determined by a balance among the interfacial energies, as well as torque terms resulting from the anisotropic interfacial energies. For a simplified case where the anisotropies in interfacial energies and torque terms can be neglected, the dihedral angle (θ) is given by:

$$2\gamma_{cl}\cos(\theta/2)=\gamma_{gb} \quad (1)$$

where γ_{cl} and γ_{gb} are, respectively, the (isotropic) interfacial energies for a crystal/liquid interface and a GB (Figure 1[a]). It should be noted that the γ_{cl} and γ_{gb} are generally anisotropic and their dependences on the crystallographic orientation and misorientation are often unknown, so Equation (1) is only an isotropic approximation. Moreover, kinetic limitations to thermodynamic equilibria often exist (e.g., it was assumed that a steady-state dynamic, instead of equilibrium, dihedral angle may form during the intergranular penetration of a liquid metal in the Glickman-Nathan model[18]). The existence of applied (particularly non-uniform) stresses can further complicate the situation. Note that the observed dihedral angles in the cross sections are 2D projections of the actual 3D dihedral angles.

Figure 1 illustrates an example from a prior study.[17] Figure 1(a) shows a cross section of a typical groove formed in a solid Ni that was annealed in direct contact with an equilibrium Bi-0.36Ni liquid at 700°C for 5 h and quenched. In this experiment, the start liquid (Bi-0.36Ni) was in a chemical equilibrium with Ni to ensure no overall dissolution of Ni into the liquid. The distribution of the measured dihedral angles (θs) for a specimen annealed at 700°C for 5 h is shown in Figure 1(b), where the mean was 44.7° with a standard deviation of 19.6°. The GB-to-GB variations were related to the anisotropies in both γ_{cl} and γ_{gb}, as well as the fact that the measured dihedral angles were (random) 2D projections of the true 3D dihedral angles. However, for a large number of measurements, the average dihedral angles measured in 2D cross sections should be identical to the average dihedral angle in 3D theoretically.[19] For this particular case, the average dihedral angle did not change significantly after approximately 5 h; the error bars are large (Figure 1[c]), but they in fact represent GB-to-GB variations of GBs of different characters, as well as the random projection effect. The average liquid penetration length (L) was also measured as a function of time (Figure 1[d]), which exceeded the Ni grain size and continued to increase after about 5 h (Figure 1[e]).

A wetting transition (Figure 2[a]) may occur as either a first-order or a continuous transformation with the change of a thermodynamic potential.[20] Assuming isotropic interfacial energies, a necessary

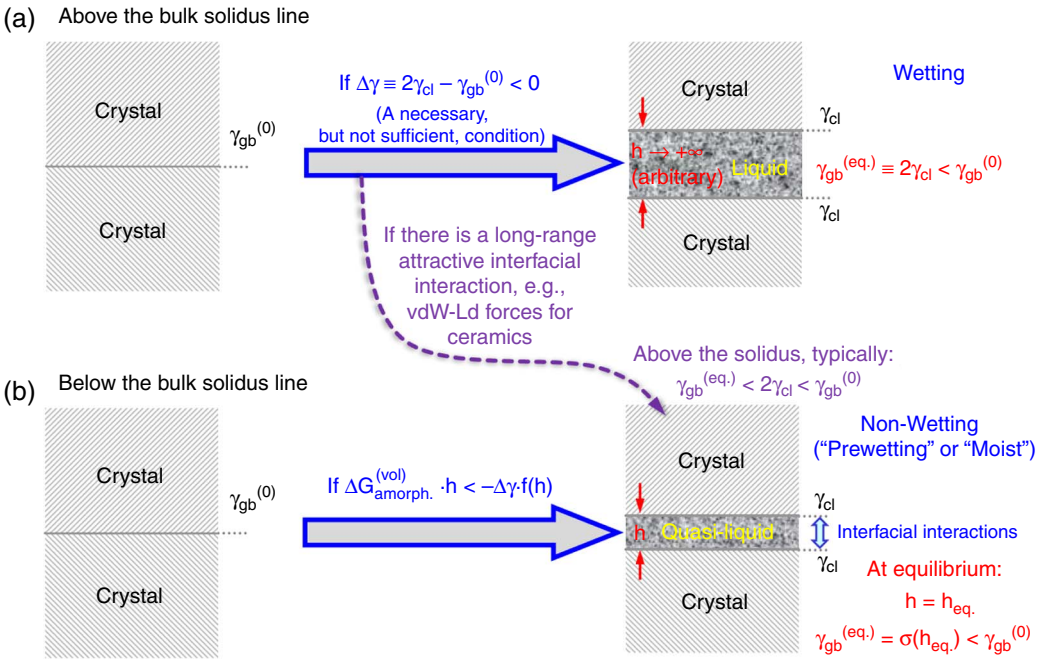

FIGURE 2. *(a) Above the bulk solidus line, a liquid film can wet a GB, where a "clean" GB is replaced by two crystal/liquid interfaces spontaneously at equilibrium. One example of GB wetting is shown in Figure 3(b). (b) Below the bulk solidus line, a quasi-liquid film (liquid-like GB complexion) of a nanoscale thickness h can be thermodynamically stabilized at a GB if the interfacial energy reduction ($-\Delta\gamma$) is greater than the free-energy penalty for forming the undercooled liquid film ($\Delta G_{amorph.}^{(vol)} \cdot h$). This explains the thermodynamic stabilization of the liquid-like GB complexion in Ni-doped Mo below the bulk solidus line, as shown in Figure 3(c). In panel (b), the quasi-liquid interfacial film (complexion) will adopt an "equilibrium" thickness at a thermodynamic equilibrium. It shall also be noted that analogous equilibrium-thickness IGFs can also be stabilized above the bulk solidus lines, particularly at ceramic GBs where the film thickness is limited by the attractive and significant vdW-Ld interactions. These equilibrium-thickness quasi-liquid IGFs (or other more ordered GB complexions), regardless whether they form above or below the bulk solidus lines/curves, represent cases of non-wetting (or "moist" in Cannon's definition; see text), even if they cover GBs continuously.*

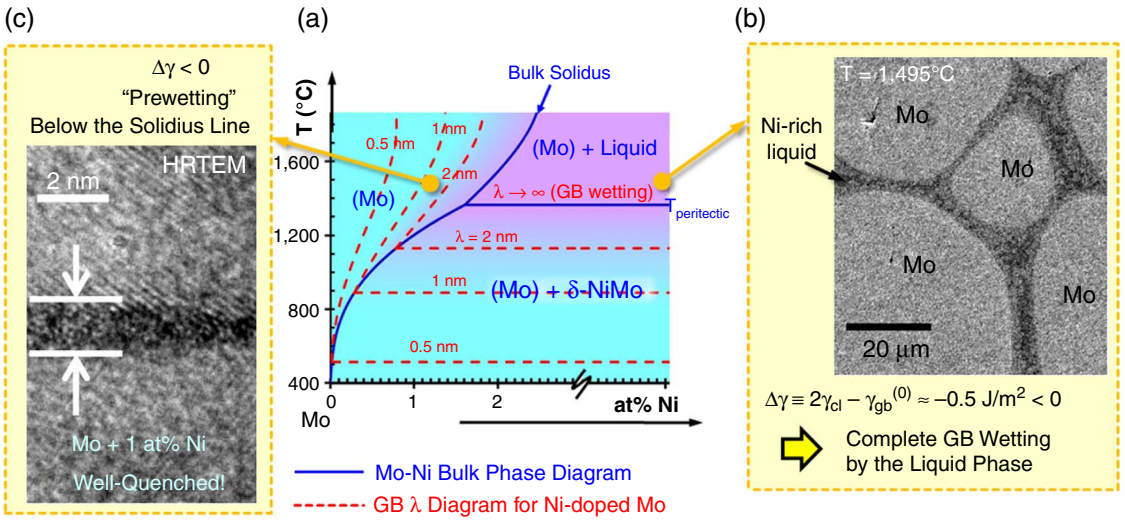

FIGURE 3. *(a) The Mo-Ni binary bulk phase diagram (and a computed "GB λ diagram" for Ni-doped Mo; see explanation below), where the solid blue lines represent bulk phase boundaries. (b) Complete GB wetting in the solid-liquid two-phase region above the bulk peritectic temperature, and (c) GB prewetting (coupled with premelting) in the single-phase region below the bulk solidus line, where Ni-enriched, nanometer-thick, liquid-like complexions are stabilized at Mo GBs when the liquid phase is not yet a stable bulk phase. In panel (a), the red dashed lines (computed λ values) represent estimated widths of the liquid-like GB complexions; thus panel (a) is also a computed "GB λ diagram" for average general GBs in Ni-doped Mo, where the colors represent the thermodynamic tendency for average general GBs to disorder (see the text and a recent review[87] for further explanation and discussion about "GB λ diagrams"). Re-plotted after Shi and Luo,* Appl. Phys. Lett. *94 (2009): p. 251908,[21] and Shi and Luo,* Phys. Rev. B *84 (2011): p. 014105,[67] with permission.*

(but not sufficient) condition for the occurrence of complete GB wetting is:

$$\gamma_{gb}^{(0)} > 2\gamma_{cl} \quad (2)$$

which is illustrated in Figure 2(a). Here, the superscript "(0)" in $\gamma_{gb}^{(0)}$ refers to a hypothetic "clean" GB without any adsorption of the liquid species; at a thermodynamic equilibrium, however, this hypothetic $\gamma_{gb}^{(0)}$ is replaced by $2\gamma_{cl}$. Thus, by definition, the equilibrium GB energy for a wetted GB is given by:

$$\gamma_{gb} \equiv \gamma_{gb}^{(eq.)} = 2\gamma_{cl} \quad (3)$$

In fact, Equation (3) (instead of Equation [2]) is a necessary and sufficient condition for the occurrence of complete GB wetting, though it is not practically useful for judging whether GB wetting would occur. One example of the wetting of Mo GBs by a Ni-rich liquid (with equilibrium composition on the liquidus line) is shown in Figure 3(b).[21] Other examples of GB wetting are demonstrated for Cu-In,[22] Al-Sn,[23] Al-Zn, and Zn-Al[24] systems, where the primary phases are underlined.

It should be pointed out that Equations (2) and (3) are isotropic approximations for GB wetting, which may be used to assess the behaviors of average general GBs (whereas special, high-symmetry GBs typically behave differently). GB character, as well as the anisotropy in γ_{cl}, can often cause significant GB-to-GB variations in the individual wetting temperatures/conditions in a polycrystalline specimen; some examples were given in an earlier review by Straumal and Baretzky.[25]

Finally, it is imperative to emphasize again that Equation (2) by itself is not a sufficient condition for the occurrence of GB wetting. For example, a recent study[17] demonstrated that although $\gamma_{gb}^{(Ni,0)} > 2\gamma_{cl}$ in the Ni-Bi binary system, the Bi-rich liquid does not completely wet the Ni GB, as shown in Figure 1. This is because the adsorption of Bi significantly reduces the GB energy ($\gamma_{gb}^{(Ni-Bi,eq.)} \approx 1/4 \times \gamma_{gb}^{(Ni,0)}$ based on a prior estimation[17]) so that at the chemical (thermodynamic) equilibrium:

$$\gamma_{gb}^{(Ni-Bi,eq.)} = 2\gamma_{cl}\cos(\theta/2)2\gamma_{cl} \quad (4)$$

where the mean θ was measured to be ~44.7° (Figure 1), so that a complete wetting does not occur (as $\gamma_{gb}^{(Ni-Bi,eq.)} < 2\gamma_{cl} < \gamma_{gb}^{(Ni,0)}$).[17] Yet, another similar (non-wetting) case is represented by the nanoscale, equilibrium-thickness, intergranular films (IGFs) (see elaboration in the *Equilibrium Intergranular Films Versus Coupled Grain Boundary Prewetting and Premelting* section and Luo[26]) that formed ubiquitously in ceramic materials above (as well as below) the bulk solidus lines/curves,[26] where the film thickness is often limited by the presence of attractive long-range van der Waals London dispersion (vdW-Ld) interactions above the solidus lines/curves at ceramic GBs; here it is again expected that $\gamma_{gb}^{(eq.)} < 2\gamma_{cl} < \gamma_{gb}^{(0)}$ in typical cases

above the bulk solidus lines (Figure 2). Thus, these equilibrium-thickness IGFs are also considered as "non-wetting" thermodynamically, despite that the nanoscale IGFs cover the GBs continuously (and Equation [2] is satisfied); see the *An Example of Generalized Grain Boundary Prewetting in Ni-Doped Mo* and *Equilibrium Intergranular Films Versus Coupled Grain Boundary Prewetting and Premelting* sections for further elaboration. Hence, it is emphasized that $\gamma_{gb}^{(eq.)} = 2\gamma_{cl} < \gamma_{gb}^{(0)}$ for a case of complete wetting in Figure 2(a), according to Equations (2) and (3).

PREWETTING AND COMPLEXION TRANSITIONS

An Example of Generalized Grain Boundary Prewetting in Ni-Doped Mo

In the prior section, it is emphasized that the wetting phase should be arbitrarily thick for the case of complete wetting. In contrast, a GB can be continuously covered by a nanometer-thick quasi-liquid interfacial film of a thermodynamically-determined "equilibrium" thickness[14] (aka a "non-autonomous 2D interfacial phase" defined by Defay and Prigogine[27] or a liquid-like "complexion," as discussed further in the *A Broader Perspective: Grain Boundary Phase-Like Transitions and Complexions* section) below the bulk solidus line, where the liquid is not yet a stable (equilibrium) bulk phase, as illustrated in Figure 2(b). A real example of such a case is shown Figure 3(c), where nanometer-thick, Ni-based, liquid-like films are stabilized at Mo GBs below the bulk solidus line, where the bulk liquid phase is not yet stable (see Figure 3).[26,28] Again, this is not a case of (complete or perfect) wetting; however, it may be considered as a case of generalized prewetting[29] (coupled with premelting, as discussed further in the *Premelting in Unary Systems* and *Equilibrium Intergranular Films Versus Coupled Grain Boundary Prewetting and Premelting* sections), which was also called "moist"—intermediate to "wet" and "dry"—by the late Dr. Rowland Cannon.[30-31]

In a broad definition, (generalized) prewetting transitions refer to wetting transitions occurring when the phases that do the wetting are not yet stable bulk phases.[20] To explain the case shown in Figure 3(c) in a phenomenological theory, a Ni-enriched, quasi-liquid film may appear and cover a Mo GB continuously below the bulk solidus line, if:

$$-\Delta\gamma \equiv (\gamma_{gb}^{(0)} - 2\gamma_{cl}) > \Delta G_{amorph.}^{(vol)} \cdot h \qquad (5a)$$

where $\Delta G_{amorph.}^{(vol)} \cdot h$ is the volumetric free-energy penalty for forming the metastable, undercooled, Ni-enriched, quasi-liquid film of a nanoscale effective interfacial width (thickness) of h (Figure 2[b]). It shall be further noted that when the film thickness (h) is of the order of 1 nm or lower, the two crystal/liquid interfaces are no longer independent and the film becomes "quasi-liquid" because of the partial orders imposed by adjacent crystalline grains. Consequently, effective interfacial interactions arise, so that Equation (5a) should be revised as:

$$-\Delta\gamma \cdot f(h) > \Delta G_{amorph.}^{(vol)} \cdot h \qquad (5b)$$

where f(h) is the dimensionless interfacial coefficient (with the following boundary conditions: f(0) = 0 and f (+∞) = 1 by definition) that represents the effects of all (thickness-dependent) interfacial interactions. This proposed stabilization mechanism is schematically illustrated in Figure 2(b).

Prewetting adsorption transitions in binary demixed liquids were first discussed in the famous critical point wetting model by Cahn in 1977.[29] Figure 3(c) can be considered as a generalized case of GB prewetting occurring in the single body-centered cubic phase region below the bulk solidus line, where prewetting adsorption occurs in conjunction (and coupled) with interfacial disordering (premelting).

Premelting in Unary Systems

The case illustrated in Figure 3(c) is in fact a case of coupled prewetting and premelting in a binary alloy. Here, premelting refers to the stabilization of a quasi-liquid interfacial film at conditions that a bulk liquid phase is thermodynamically unstable. Michael Faraday initially proposed the "surface melting" or "premelting" of ice below 0°C in the middle 19th century, which was subsequently confirmed for ice by extensive experiments and modeling, as well as observed for other unary solids such as lead.[32-34]

To some extent, premelting can be considered as a special case of prewetting, where the (pre)wetting phase is the unstable liquid below the bulk melting temperature. The term premelting is rigorously defined for unary systems; it emphasizes the interfacial structural disordering (whereas the term prewetting is sometime used to emphasize interfacial adsorption/chemical transitions).

GB premelting has been modeled by atomistic simulations by many researchers.[35-42] In the 1980s, experimental materials scientists had also sought to confirm the existence of GB premelting in unary materials. In 1989, Balluffi's group reported that GB premelting did not occur up to $0.999T_{melting}$ for pure Al,[43] which greatly discouraged further experimental exploration in this field. In 2005, GB premelting was discovered in a colloidal crystal.[44] Nonetheless, the significance and importance of GB premelting in real unary materials remains controversial.

Equilibrium Intergranular Films Versus Coupled Grain Boundary Prewetting and Premelting

In the ceramics community, researchers have long recognized the widespread existence of a unique

class of impurity-based, equilibrium-thickness, intergranular films or IGFs at ceramic GBs and hetero-phase boundaries (see *Critical Reviews*[26] and references therein). These nanoscale IGFs can be alternatively and equivalently understood to be: (1) liquid-like interfacial films that adopt an "equilibrium" thickness of the order of 1 nm in response to several attractive and repulsive interfacial forces acting on the film (the Clarke model)[45-46] or (2) a unique class of disordered multilayer adsorbates with average film composition set by bulk chemical potentials (the Cannon model).[30] More recently, metallic counterparts (e.g., Figure 3[c])[21,47-48] and free-surface counterparts[28,49-58] to these ceramic IGFs have also been observed, showing the widespread existence of analogous 2D interfacial phases. Interestingly, these impurity-based, quasi-liquid interfacial films have been found to form below the bulk solidus lines,[21,26,28,47-48,59-61] provoking an analogy to the phenomenon of premelting in unary systems.

A series of recent studies suggested that a class of premelting-like interfacial films can be stabilized at GBs over wider ranges of undercooling in multicomponent materials, wherein GB disordering is enhanced by a concurrent GB segregation (aka adsorption). In 2006, Tang, Carter, and Cannon[62] explained the formation of subsolidus IGFs in binary systems from coupled GB premelting (structural disordering) and prewetting (chemical adsorption) transitions[62] using a diffuse-interface (phase-field) model extended from the Cahn critical-point-wetting model,[29] which was further elaborated by Mishin, et al.[63] As prior indirect measurements already indicated the occurrence of GB premelting-like transitions in certain metallic systems (e.g., Fe-Si-Zn),[25,64-66] more recent studies further provided the direct high-resolution transmission electron microscopy (HR-TEM) evidence for the existence of premelting-like quasi-liquid IGFs below the bulk solidus lines in metallic alloys (e.g., in Mo-Ni system as shown in Figure 3[c] and W-Ni system).[21,47,60,67-68]

A Broader Perspective: Grain Boundary Phase-Like Transitions and Complexions

GB premelting and prewetting (discussed in the previous section) can be considered as the representative GB structural and adsorption transitions, respectively. In 1968, Hart had already proposed that GBs can be considered as "2D interfacial phases" that may undergo "phase" transformations.[69-70] Subsequent models developed by Hondros and Seah,[71-72] Cahn,[29,73-75] Clarke,[45-46] Carter, et al.,[62,76-78] Wynblatt and Chatain,[79-80] Mishin, et al.,[63,81-84] and Luo, et al.,[16,85-87] further elaborated this concept. The occurrence of first-order GB transitions was also evident in Si-Au[88] and TiO_2-CuO-SiO_2.[89]

Tang, Carter, and Cannon[62,76] named such 2D interfacial phases as "complexions" based on an argument that they not "phases" according to the rigorous Gibbs definition because they have no identifiable volume and cannot exist without abutting bulk phases. In this regard, complexions are essentially the "non-autonomous phases" defined by Defay and Prigogine in early literature.[27]

In 2007, Dillon and Harmer[90-93] reported the discovery of a series of six discrete GB complexions in doped Al_2O_3 (Figure 4[a]). Recent studies[14-16,21,67-68,88] further revealed the existence of this series of Dillon-Harmer complexions in metals (Figure 4[b]). To some extent, this series of Dillon-Harmer complexions can be considered as derivatives of IGFs with discrete thickness of 0, 1, 2, 3, x, and ∞ atomic layers, respectively.

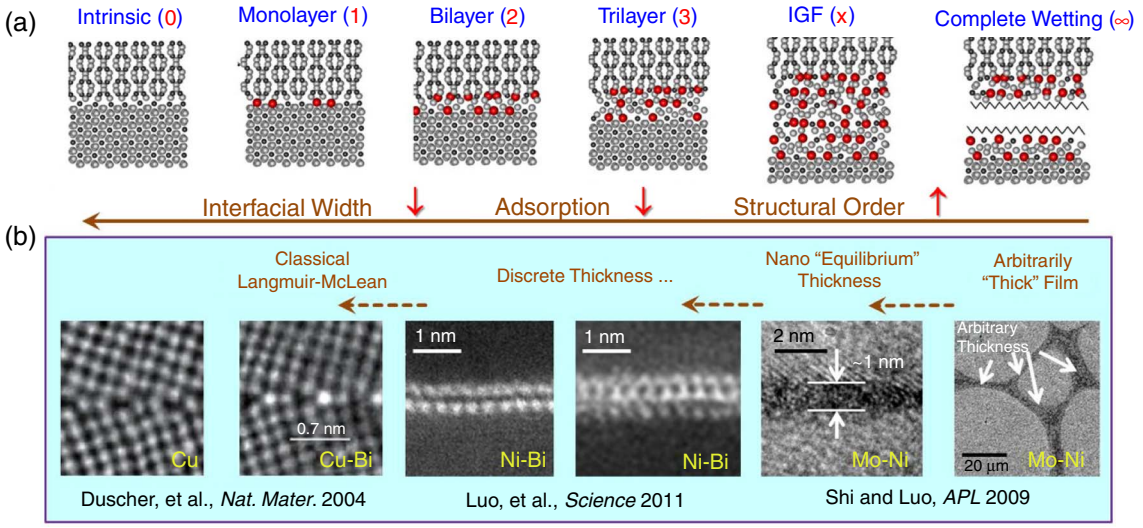

FIGURE 4. *A series of 2D interfacial phases at GBs (Dillon-Harmer complexions) were observed in (a) doped Al_2O_3,[91] and (b) various metals.[16,21,47,104] This series of Dillon-Harmer complexions can be considered as IGFs with discrete thickness of 0, 1, 2, 3, x, and ∞ atomic layers, respectively. Reprinted from Luo, et al.,* Science *333 (2011): p. 1730-1733,[16] with permission.*

These findings and theories of GB complexions and transitions provide new insights for understanding the atomic-level mechanisms for solid-state activated sintering,[47,60,67,85,87,94-95] abnormal grain growth,[90-92,96] and LME,[15-16] each of which has puzzled the materials science community for more than half a century.

This emerging research area has recently been reviewed by Cantwell, et al.,[14] and by Kaplan, Chatain, Wynblatt, and Carter.[78]

Development of Grain Boundary Diagrams as a New Materials Science Tool

As shown in Figure 2(b) and Equation (5), a quasi-liquid IGF can be thermodynamically stabilized. In a sharp-interface model, the relative interfacial energy can be expressed as:

$$\sigma(h) - \sigma(0) \equiv \Delta\gamma \cdot f(h) + \Delta G^{(vol)}_{amorph.} \cdot h \qquad (6)$$

where $\sigma(0) \equiv \gamma^{(0)}_{gb}$ by definition. Subsequently, a thermodynamic variable, λ, was defined to represent the maximum thickness of a quasi-liquid interfacial film that can be stabilized at an average GB without consideration of interfacial interactions:

$$\lambda \equiv Max[-\Delta\gamma/\Delta G^{(vol)}_{amorph.}] \qquad (7)$$

The computed λ value represents the thermodynamic tendency to stabilize a quasi-liquid IGF at an average general (random) GB, and it scales the actual interfacial width (which, in this sharp-interface model, corresponds to the global minimum in Equation [6] that corresponds to an "equilibrium" thickness $h_{eq.}$ and equilibrium GB energy $\gamma^{(eq.)}_{gb} = \sigma(h_{eq.}) < \gamma^{(0)}_{gb}$; see Figure 2[b]). Subsequently, λ and plot lines of constant λ in bulk phase diagrams can be quantified to construct a new kind of "GB λ diagrams." An example is shown in Figure 3(a) for Ni-doped Mo.

The correctness and usefulness of these GB λ diagrams have been systematically validated by experiments. First, the model predictions were corroborated with direct HR-TEM and Auger electron spectroscopy analysis (see Figure 3 for an example).[21,47,60,67,85] Second, the computed GB λ diagrams (with no free parameters) correctly predicted the onset sintering temperatures, as well as trends in sintering rates for binary[67,85,95] and multicomponent[97] alloys. Third, the predicted GB solidus temperature was consistent with a prior direct GB diffusivity measurement for W-Co using radioactive tracers.[85,98] Moreover, the estimated GB diffusivity as a function of temperature and overall composition for Mo-Ni correlated well with the computed binary GB λ diagram.[67] Most interestingly, a counterintuitive phenomenon of decreasing GB diffusivity with increasing temperature predicted by the computed GB λ diagram of the Mo-Ni system was subsequently verified experimentally for a Mo + 0.5 at% Ni alloy.[68]

It is emphasized that these GB λ diagrams, such as the one shown in Figure 3(a), represent the thermodynamic tendency for *average* general GBs to disorder, while the GB-to-GB variations for general GBs should and have also been estimated, see, e.g., Luo.[87,95] However, special GBs usually need to be treated case by case, which are not considered in this model. Furthermore, this model does not consider the possible faceting resulting from the anisotropy in interfacial energies and its consequence.

These GB λ diagrams, although they can predict useful trends, are not yet rigorous GB "phase" (complexion) diagrams. Current studies are in progress to develop rigorous GB complexion (phase) diagrams with well-defined transition lines and critical points. It is expected that both the GB λ diagrams and rigorous GB complexion diagrams can generate useful trends to help understand and control LME and LMC, as well as many other materials properties by avoiding temperatures and chemical environments where detrimental GB complexions may form. Or, they can be used to find the suitable doping/alloying strategies and heat treatment protocols to control and adjust GB structures and chemistry to remediate embrittlement or improve corrosion resistance and other material properties.

As bulk phase diagrams are among the most useful tools for designing materials processing and properties, it is expected that GB "phase" (complexion) diagrams can be an equally-important tool for use in materials science in general, as well as for understanding and controlling LME and LMC specifically.

LIQUID METAL EMBRITTLEMENT IN NI-BI AND CU-BI

Intrinsically ductile metals, such as Ni, Cu, and Fe, are prone to catastrophic failure when exposed to certain liquid metals.[4-11] Specifically, Ni-Bi and Cu-Bi are model LME systems, where it was well established that the adsorption of Bi at Ni or Cu GBs in front of the penetration tips embrittled the GBs.[4,99-101] However, the exact atomic level mechanism of this LME phenomenon in Ni-Bi and Cu-Bi has been the subject of scrutiny and debate for decades.

A recent experimental study revealed the formation of Bi-based bilayer adsorption as the origin of LME in Ni-Bi (Figure 5[a]).[16] This underlying embrittlement mechanism is somewhat similar to how soap molecules separate grease from a surface. Basically, Bi atoms penetrate into GBs of Ni to form bilayer adsorption, with one monolayer of Bi adsorbates strongly bonded to each of the two grain surfaces, whereas the two adsorbed Bi monolayers are weakly bonded to each other, leading to extremely low GB cohesion. Two subsequent independent studies of

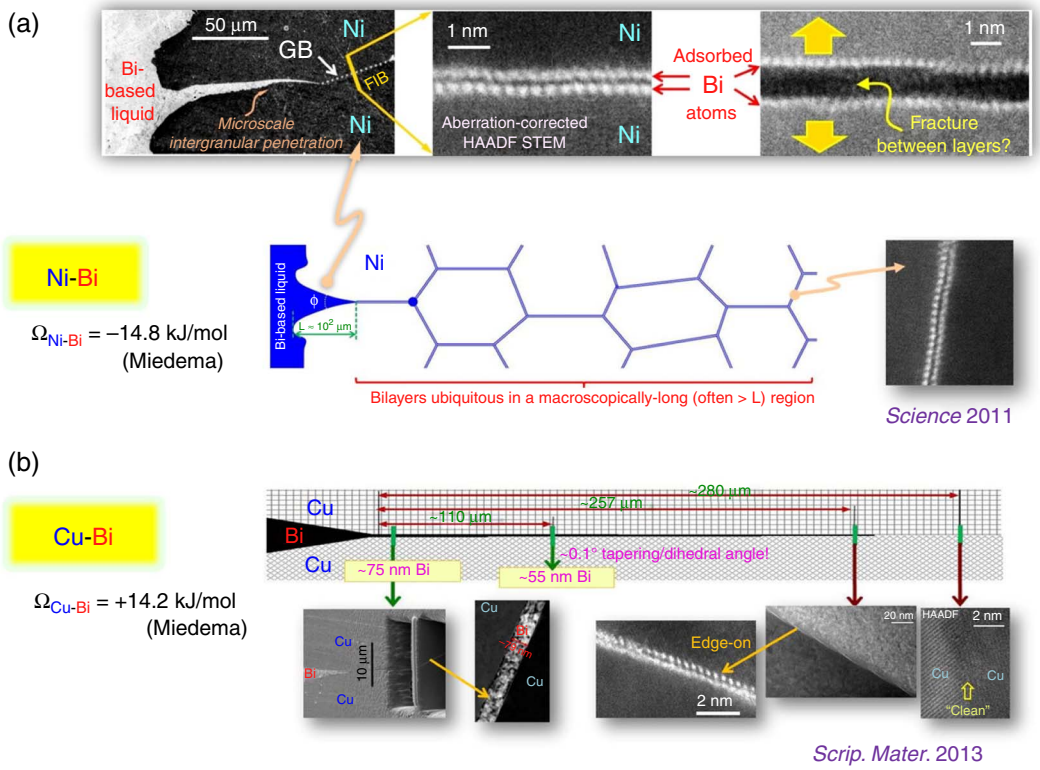

FIGURE 5. *(a) Bi-based bilayers formed at Ni general GBs; weak cohesion between Bi adsorbate layers, each of which are strongly bonded to the abutting grain surfaces, is the root cause of LME in Ni-Bi. (b) Comparison of Ni-Bi vs. Cu-Bi systems. While the bilayers are ubiquitous in Ni-Bi, they only exist in a small Bi chemical potential window in Cu-Bi, in front of a very long, nearly-wetting, Bi-based liquid film. The difference in the bilayer stability can be well explained by different mixing enthalpies of the two systems, where a significant negative mixing enthalpy for Ni-Bi favors the formation of bilayers. Re-plotted after Kundu, et al.,* Scrip. Mater. *68 (2013): p. 146-149,[15] and Luo, et al.,* Science *333 (2011): p. 1730-1733,[16] with permission.*

quantum-mechanical density functional theory (DFT) calculations further supported this proposed mechanism.[102-103]

Bilayers were also observed in Cu-Bi (Figure 5[b]).[15] A comparison of Ni-Bi and Cu-Bi offers further insights. While bilayers are ubiquitous in Ni-Bi, they only exist in a small Bi chemical potential window in Cu-Bi, in front of a long, nearly wetting, Bi-based liquid film (Figure 5[b]). This difference in the bilayer stability can be explained by the different mixing enthalpies (Figure 5[b]), where a large negative mixing enthalpy for Ni-Bi favors the formation of bilayers.[15-16]

In a broader perspective, the studies of LME in Ni-Bi and Cu-Bi strikingly demonstrated that adsorption (GB segregation) can induce a GB phase-like (complexion) transition that causes drastic changes in properties.[15-16] LME is a special (severe) case of GB embrittlement.[104-107] All three classical GB embrittlement models were discussed mostly based on the McLean-Langmuir type segregation model, where the reduction of GB cohesion was explained by an electronic effect,[104,106] an atomic-size-difference (strain) effect,[105] or the changes in relative interfacial energies (the Rice-Wang model).[108] In addition to the observations of bilayers in Ni-Bi and Cu-Bi (Figure 5),[15-16] disordered (glass-like) nanoscale IGFs have been observed directly by HR-TEM for two GB embrittlement systems, i.e., W-Ni and Mo-Ni (see, e.g., Figure 3[c]), where the embrittlement mechanisms may be related to the general brittleness of metallic glass (or, presumably, metallic glass-like complexions).[21,47] These results collectively point one toward revisiting GB embrittlement models to consider the effects of GB complexion (particularly structural) transitions.

CO-DOPING EFFECTS ON GRAIN BOUNDARY PENETRATION AND LIQUID METAL CORROSION

The development of GB grooves (Figure 1) has been studied in the context of two related materials phenomena—LME as discussed in the prior section and LMC.[1,109-113] LMC (as well as LME) is technologically important for understanding and controlling hot dip galvanization, welding, soldering, and the safety of liquid metal cooled nuclear reactors.[1,109-113] LMC studies focus on the dissolution at the solid/liquid

interfaces, where preferential intergranular dissolution and penetration are often the dominating corrosion processes.

Specifically, the impurity effects on LMC have been investigated in the context of seeking corrosion inhibitors, e.g., the addition of Zr and Ti can significantly inhibit the LMC of carbon and low alloy steels in the Pb-Bi liquid, but it does not have considerable effects for the stainless steels.[1,3,109-110] These corrosion inhibitors prevent the dissolution of solids by promoting the formation of the protective oxide layers on the solid surfaces.

This section reviews a recent study[17] of the intrinsic impurity/co-doping effect on LMC without surface native oxide layers, which is practically important because it represents the late stage of corrosion after breaking the native oxides[113] but has not been systematically investigated prior to 2012. In general, investigating the impurity effects on intergranular penetration is important because the presence of impurities or internally added alloying elements is prevailing. Moreover, understanding the impurity effects can offer a new route to control LMC via alloying.

Using Ni-Bi as the model system, this recent study[17] demonstrated significant enhancements of intergranular liquid metal penetration and LMC upon adding small amounts of impurities in either the solid or the liquid (Figure 6). Specifically, a variety of intergranular penetration kinetics and morphologies were observed and explained via the interplay of interfacial segregation, wetting, various bulk phase transformations, and stress generation. The key results are summarized as follows.

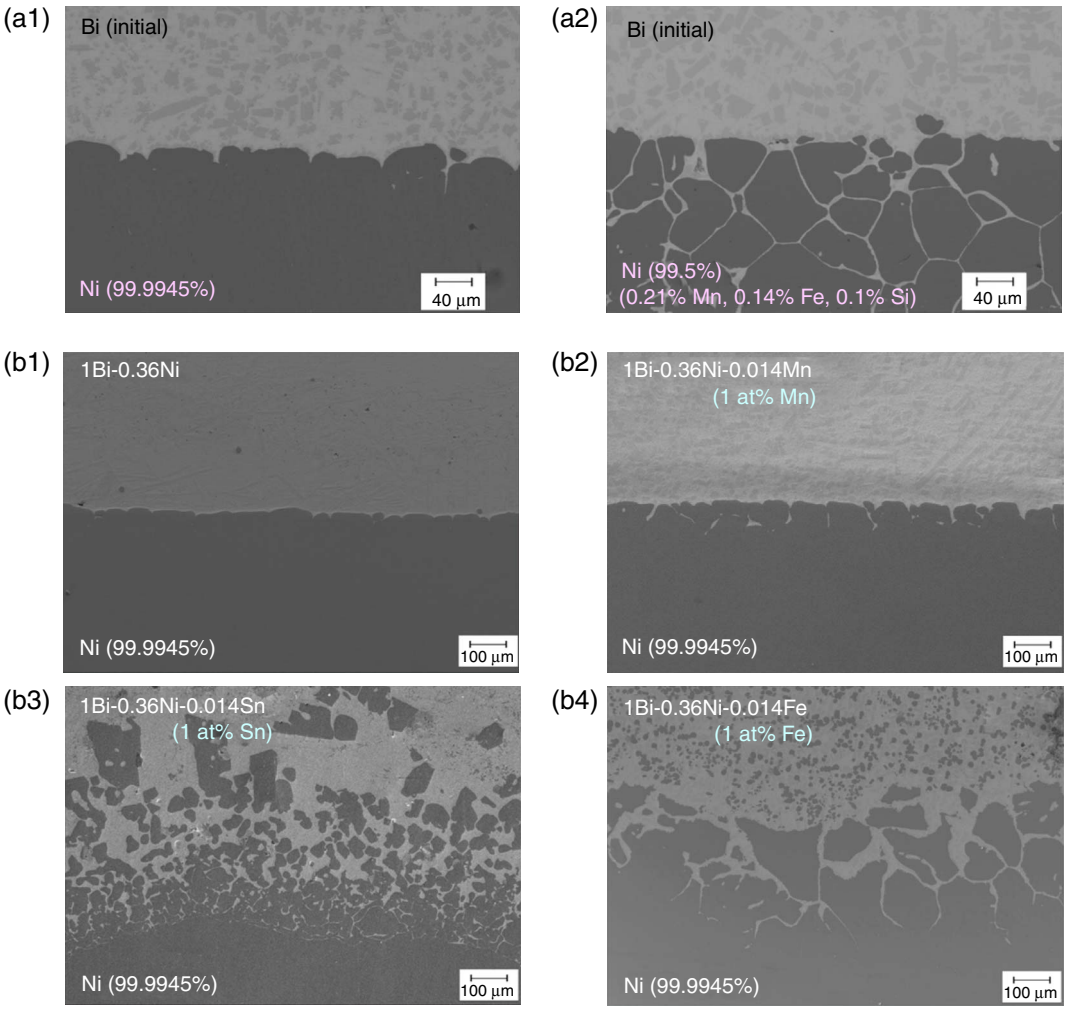

FIGURE 6. *SEM cross-sectional images of (a1) a pure (99.9945 at% Ni) specimen and (a2) an impure specimen (in at%: 99.5 Ni, 0.21 Mn, 0.14 Fe, and 0.1 Si) of similar average grain sizes of ~75 μm after annealing in contact with initially pure Bi liquids at 700°C for 5 h. (b1) through (b4) The effects of the addition of impurities in the liquid on the intergranular penetration of pure (99.9945 at%) Ni. Representative cross-sectional SEM images for specimens penetrated by (b1) a Bi + 0.36Ni liquid without other impurities (as the reference) vs. Bi-0.36Ni liquids with the addition of 1 at% of (b2) Mn, (b3) Sn, and (b4) Fe, respectively. The initial liquid compositions are labeled. All specimens were annealed at 700°C for 5 h. Re-plotted after Asl and Luo,* Acta Mater. *60 (2012): p. 149-165,[17] with permission from Elsevier.*

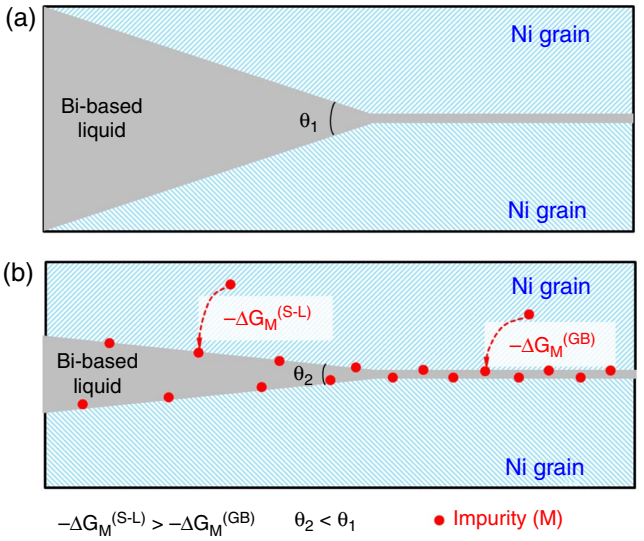

FIGURE 7. *Schematic illustration of the proposed mechanism for the observed impurity enhanced the intergranular penetration. The adsorption of the impurity/co-doping elements will reduce crystal/liquid interfacial energy more than the GB energy, leading to a reduction in the dihedral angle that subsequently enhances intergranular penetration. Reprinted from Asl and Luo,* Acta Mater. *60 (2012): p. 149-165,[17] with permission from Elsevier.*

First and foremost, the presence of minor impurities (in either the solid or the liquid) can significantly enhance the intergranular penetration (Figure 6). For example, <0.5 at% total impurities in the solid Ni could increase the penetration length by six times.[17]

Second, a new analytical model has been derived for the impurity/co-doping effect on changing the equilibrium dihedral angle for the dilute solution limit, which subsequently enhances the penetration kinetics. Interested readers are referred to Asl and Luo[17] for the details of this model; the key concept is illustrated in Figure 7, where adsorption of an impurity can reduce the solid/liquid interfacial energy ($2\gamma_{cl}^{(eq.)}$) faster than the GB energy ($\gamma_{gb}^{(eq.)}$) because the segregation energy is generally more negative at the solid/liquid interface ($-\Delta G_M^{(GB)} < -\Delta G_M^{(S-L)}$, as shown in Figure 7). This should reduce the average equilibrium dihedral angle ($\theta_2 < \theta_1$ in Figure 7) to further enhance the intergranular penetration based on the well-established LMC models (the Mullins model[114-115] and the Glickman-Nathan model[18]). For example, the penetration length would increase by 4.7 times if the average equilibrium dihedral angle θ was reduced from ~44.7° to 10°, which is consistent with the experimental observation.[17]

This key concept in this model followed a similar idea proposed in the Rice-Wang model[108] for GB embrittlement, where they proposed that the reduction in GB cohesion is because the surface segregation energy is greater in magnitude (more negative) than the corresponding GB segregation energy. A similar mechanism was also used by Glickman[116] to explain the "alloying effect" in enhancing stress corrosion cracking, and by Zhang and Luo[12] to explain the triple-line instability in Ni-Bi-S system; the latter case is discussed in the next section.

Furthermore, when the initially pure Bi was applied, the intergranular penetration could be enhanced as a result of a dissolution effect, and this enhancement could be magnified when it interacted with the impurity effects. This is strikingly shown in the comparison of Figures 6(a1) vs. (a2).

Finally, effects of adding three specific co-dopants (Mn, Sn, and Fe) on the LMC of Ni-Bi are briefly summarized as follows (see Figures 6[b1] through [b4] for a comparison; more details can be found in Asl and Luo[17]):

- Mn or Sn co-dopants (initially added to the liquid) were rejected from the liquid and dissolved and diffused into solid Ni grains, generating compressive strains and leading to different intergranular wetting and penetration morphologies (Figures 6[b2] and [b3] vs. [b1]).
- Because the interfacial segregation of Mn is moderate, adding a small amount of Mn only enhanced intergranular penetration moderately (Figure 6[b2]), while adding a large amount of Mn enhanced the penetration significantly more (see Asl and Luo[17]).
- In contrast, adding a small amount of strong segregating element Sn already enhanced the penetration significantly (Figure 6[b3]), but adding a large amount of Sn did not enhance the penetration much further (see Asl and Luo[17]) because segregation already reached the saturation levels.
- Fe co-dopants precipitated out as solid particles, which consumed some Ni from the liquid and drove the Ni to be dissolved to the liquid from the Ni grains. This dissolution process significantly enhanced intergranular penetration even if Fe only segregates weakly. This different mechanism resulted in rough solid/liquid interfaces and the tapering of the intergranular liquid channels (Figure 6[b4]).

The basic concepts and framework developed in that study[17] (and summarized above) can be generalized to understand the impurity effects on LMC in other materials systems.

TRIPLE-LINE WETTING

When the interfacial energies can be assumed to be isotropic for simplicity, Equation (3) indicates the occurrence of GB wetting when the γ_{gb}/γ_{cl} ratio is two. Moreover, in an isotropic approximation, triple-grain junctions can be wetted by the liquid phase if:

$$\frac{\gamma_{gb}}{\gamma_{cl}} > \sqrt{3} \qquad (8)$$

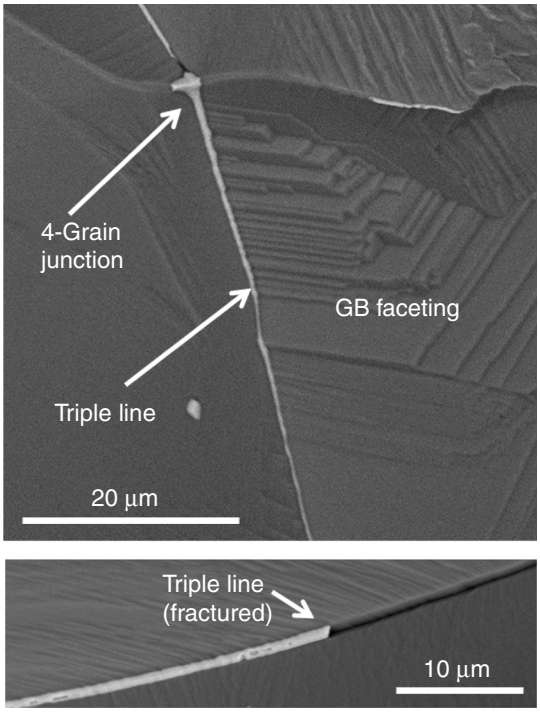

FIGURE 8. *Wetting of the triple-grain junctions by liquid phases in the LME system Ni-Bi; the images are SEM micrographs of intergranularly fractured specimens. Reprinted with revisions from the Supporting Online Materials of Luo, et al.,* Science *333 (2011): p. 1730-1733,*[16] *with permission.*

which have been observed in Ni-Bi (Figure 8),[16] W-Ni,[47] and several other systems. The occurrence of triple-line wetting is relevant to both LMC and LME as it provides fast transport pathway along the network of triple-grain junctions, which is particularly important for LMC, but can also play a significant role for LME kinetics (of forming embrittled GBs after contacting the liquid metal); moreover, cracks may also nucleate at the wetted triple junctions.

In an extreme case, triple-grain junctions can also be wetted by a gas (vapor) phase if:

$$\frac{\gamma_{gb}}{\gamma_S} > \sqrt{3} \tag{9}$$

where γ_S is the surface energy. This triple-junction wetting by a gas phase will lead to triple-line instability or the formation of holes at triple-grain junctions. This unusual phenomenon has been observed for S-doped Ni annealed in the Bi vapor (Figure 9).[12]

This unusual phenomenon of triple-line instability (Figure 9) is related to the bilayer formation in this system (Figure 5[a]), where the two adsorbed Bi layers bonded weakly; thus, a first order of approximation (see Zhang and Luo[12] for details) estimates:

$$\frac{\gamma_{gb}}{\gamma_S} \approx 2 - \frac{\Delta\gamma^{(Bi-Bi)}}{\gamma_S} \tag{10}$$

where $\Delta\gamma^{(Bi-Bi)}$ is the cohesive energy (per unit area) between two adsorbed Bi layers, which is small (as verified by two DFT calculations[102-103]) so that γ_{gb}/γ_S can be large.

Yet, unstable triple-lines were only observed in Bi and S co-doped Ni,[12] where both S and Bi are known to strongly segregate at surfaces and GBs. Analogous to the Rice-Wang model,[108] segregation of the S co-dopants will reduce $2\gamma_S$ more than γ_{gb} because the surface segregation enthalpy is generally greater in

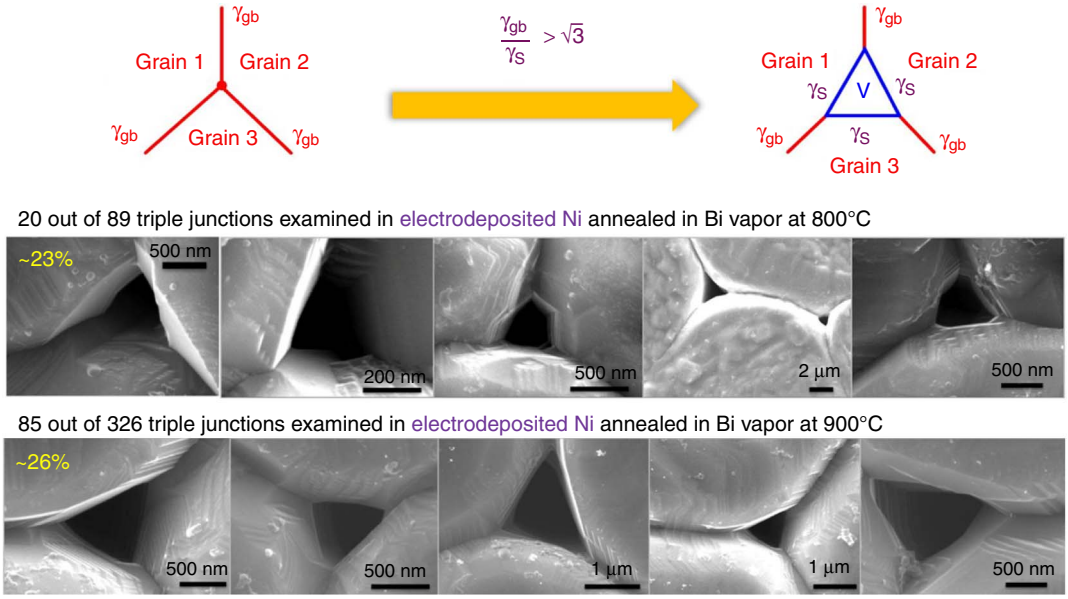

FIGURE 9. *Observation of triple-line instability for electrodeposited Ni annealed in Bi vapor, which can be explained as wetting of the triple-grain junctions by a vapor phase. Reprinted from Zhang and Luo,* Scrip. Mater. *88 (2014): p. 45-48,*[12] *with permission.*

magnitude (more negative) than GB segregation enthalpy. Thus, co-segregation of S may further increase the ratio of γ_{gb}/γ_S to $> \sim\sqrt{3}$ to induce triple-line instability. See Zhang and Luo[12] for details.

In the current case, open channels were only observed at a fraction of triple lines/junctions, which can be explained by anisotropy in the interfacial energies (both γ_{gb} and γ_S).[12]

In summary, triple-grain-line wetting by the Bi-rich liquid phase was observed for Ni-Bi (Figure 8), which can significantly impact both LMC and LME.[16] Moreover, an unusual high-temperature capillary phenomenon of triple-line instability (wetting by a gas phase to form open channels) was reported for (Bi + S) co-doped Ni (Figure 9), which is rare because it requires a critically large γ_{gb}/γ_S ratio ($> \sqrt{3}$ with an isotropic approximation). This unusual triple-line instability is likely resulted from strong interfacial segregation of both Bi and S and related to bilayer formation. This phenomenon is correlated with severe GB embrittlement, and it can significantly affect corrosion resistance in the vapor phase.

CONCLUSIONS

❖ A short review of both the history of and recent advancements in the high-temperature wetting and complexion transitions in metallic alloys has been given, with a particular focus on a critical assessment of their influence on LME and LMC. In addition to the relevant theories of 2D interfacial phases (aka complexions), the review is focused on recent studies of Ni-Bi- and Cu-Bi-based systems in several connected areas. At the atomic level, recent experimental studies revealed the formation of Bi-based bilayers in Ni-Bi and Cu-Bi, which are responsible for LME of these systems.[15-16] At the microstructural level, the presence of minor impurities or co-alloying elements can significantly enhance the intergranular penetration and corrosion, and the interplay of bulk phase transitions, interfacial segregation and wetting, transport processes, and stress generation could result in a variety of intergranular penetration behaviors and morphologies.[17] Moreover, triple-line wetting by a liquid metal were observed for Ni-Bi,[16] which can significantly affect LMC and LME. Finally, an unusual phenomenon of triple-line instability in (Bi+S) co-doped Ni;[12] this phenomenon is related to the embrittlement and corrosion caused by a gas phase (e.g., that contains Bi or S vapor). A coherent theme of this review article is to assess the previously-unrecognized roles of high-temperature adsorption, wetting, and complexion transitions in LME and LMC.

❖ Several important issues that have not been discussed in sufficient detail in this short review will also be acknowledged. First, the interfacial energies are generally anisotropic; specifically, GBs have five macroscopic degrees of freedom. Thus, the actual GB behaviors, such as the occurrence of GB wetting and complexion transitions, often depend on the GB character. Most of the discussions in this short review are about the behaviors of average general GBs, whereas the GB-to-GB variations have also been estimated (see, e.g., Luo[87,95]); moreover, special GBs may need to be treated case by case (more effectively by atomistic modeling, as compared with general GBs) and faceting transitions should also be considered. Second, this review is focused on the wetting and complexion transitions under (or near) equilibrium conditions. Practically, kinetic limitations to equilibration often exist and play important roles. Applied stresses and non-equilibrium defects caused by radiation can further complicate the situation, e.g., both complexion stability and transformation kinetics can be affected. These factors can become important for understanding the LMC and LME in liquid metal cooled nuclear reactors. Finally, this review emphasizes experimental results that are directly relevant to LMC and LME, as well as the basic underlying physical concepts (and simple theories); more in-depth discussions about the relevant (general) theories and models of wetting and complexions can be found in several prior comprehensive reviews.[14,20,53,78,87,95,117-119]

ACKNOWLEDGMENTS

This review article benefited from a number of past and current research projects in different relevant scientific and technological areas that were/are supported by the Office of Naval Research MURI program via the Lehigh University (under grant no. N00014-11-1-0678, specifically on the topics of GB embrittlement of Ni-Bi and Cu-Bi and related thermodynamic models), the National Science Foundation (under grant no. CMMI-1436305, specifically on the topics of sintering of W and modeling of related quasi-liquid IGFs in W-based alloys), the Air Force Office of Scientific Research (under grant no. FA9550-10-1-0185 for 2010-2013 on the topic of high-temperature interfacial thermodynamics for Mo-Si-B-based alloys and grant no. FA9550-14-1-0174 for 2014-2019 on the topic of controlling high-temperature ceramic GBs by electric fields), the New Energy Technology Laboratory (under grant no. DE-FE0011291 on the topic of multiscale modeling of the microstructure-dependent creep of W alloys), and a National Security Science and Engineering Faculty Fellowship (NSSEFF; under grant no. N00014-15-1-0030 for developing interfacial phase diagrams as a useful component for the Materials Genome Initiative in general).

REFERENCES

1. J. Zhang, P. Hosemann, S. Maloy, *J. Nucl. Mater.* 404 (2010): p. 82-96.
2. J. Van den Bosch, R.W. Bosch, D. Sapundjiev, A. Almazouzi, *J. Nucl. Mater.* 376 (2008): p. 322-329.

3. D. Sapundjiev, S. Van Dyck, W. Bogaerts, *Corros. Sci.* 48 (2005): p. 577-594.
4. B. Joseph, M. Picat, F. Barbier, *European Phys. J.-Appl. Phys.* 5 (1999): p. 19-31.
5. C.Q. Ye, J.B. Vogt, I.P. Serre, *Mater. Sci. Eng. A* 608 (2014): p. 242-248.
6. E. Senel, J.C. Walmsley, S. Diplas, K. Nisancioglu, *Corros. Sci.* 85 (2014): p. 167-173.
7. M. Rajagopalan, M.A. Bhatia, M.A. Tschopp, D.J. Srolovitz, K.N. Solanki, *Acta Mater.* 73 (2014): p. 312-325.
8. S.P. Lynch, *Mater. Charact.* 28 (1992): p. 279-289.
9. C.F. Old, *J. Nucl. Mater.* 92 (1980): p. 2-25.
10. M.G. Nicholas, C.F. Old, *J. Mater. Sci.* 14 (1979): p. 1-18.
11. A.R. Westwood, M.H. Kamdar, *Philos. Mag.* 8 (1963): p. 787-804.
12. Y. Zhang, J. Luo, *Scrip. Mater.* 88 (2014): p. 45-48.
13. K. Wolski, V. Laporte, *Mater. Sci. Eng. A* 495 (2008): p. 138-146.
14. P.R. Cantwell, M. Tang, S.J. Dillon, J. Luo, G.S. Rohrer, M.P. Harmer, *Acta Mater.* 62 (2014): p. 1-48.
15. A. Kundu, K.M. Asl, J. Luo, M.P. Harmer, *Scrip. Mater.* 68 (2013): p. 146-149.
16. J. Luo, H. Cheng, K.M. Asl, C.J. Kiely, M.P. Harmer, *Science* 333 (2011): p. 1730-1733.
17. K.M. Asl, J. Luo, *Acta Mater.* 60 (2012): p. 149-165.
18. E.E. Glickman, M. Nathan, *J. Appl. Phys.* 85 (1999): p. 3185-3191.
19. R.T. Dehoff, *Metallography* 19 (1986): p. 209-217.
20. D. Bonn, D. Ross, *Reports on Progress in Physics* 64 (2001): p. 1085-1163.
21. X. Shi, J. Luo, *Appl. Phys. Lett.* 94 (2009): p. 251908.
22. B. Straumal, T. Muschik, W. Gust, B. Predel, *Acta Metall. Mater.* 40 (1992): p. 939-945.
23. B.B. Straumal, W. Gust, D.A. Molodov, *Interf. Sci.* 3 (1995): p. 127-132.
24. B.B. Straumal, A.S. Gornakova, O.A. Kogtenkova, S.G. Protasova, V.G. Sursaeva, B. Baretzky, *Phys. Rev. B* 78 (2008): p. 054202.
25. B.B. Straumal, B. Baretzky, *Interf. Sci.* 12 (2004): p. 147-155.
26. J. Luo, *Critical Reviews in Solid State and Material Sciences* 32 (2007): p. 67-109.
27. R. Defay, I. Prigogine, *Tension Superficielle et Adsorption* (Éditions Desoer, Liège, 1951).
28. J. Luo, Y.-M. Chiang, *Annu. Rev. Mater. Res.* 38 (2008): p. 227-249.
29. J.W. Cahn, *J. Chem. Phys.* 66 (1977): p. 3667-3672.
30. R.M. Cannon, M. Rühle, M.J. Hoffmann, R.H. French, H. Gu, A.P. Tomsia, E. Saiz, *Ceramic Transactions (Grain Boundary Engineering in Ceramics)* 118 (2000): p. 427-444.
31. R.M. Cannon, L. Esposito, *Z. Metall.* 90 (1999): p. 1002-1015.
32. J.G. Dash, *Contemporary Physics* 30 (1989): p. 89-100.
33. J.G. Dash, H. Fu, J.S. Wettlaufer, *Reports on Progress in Physics* 58 (1995): p. 115-167.
34. J.G. Dash, A.M. Rempel, J.S. Wettlaufer, *Reviews of Modern Physics* 78 (2006): p. 695-741.
35. T. Nguyen, P.S. Ho, T. Kwok, C. Nitta, S. Yip, *Phys. Rev. Lett.* 57 (1986): p. 1919-1922.
36. S.J. Fensin, D. Olmsted, D. Buta, M. Asta, A. Karma, J.J. Hoyt, *Phys. Rev. E* 81 (2010): p. 031601.
37. J.J. Hoyt, D. Olmsted, S. Jindal, M. Asta, A. Karma, *Phys. Rev. E* 79 (2009): p. 020601.
38. A. Adland, A. Karma, R. Spatschek, D. Buta, M. Asta, *Phys. Rev. B* 87 (2013): p. 024110.
39. P.L. Williams, Y. Mishin, *Acta Mater.* 57 (2009): p. 3786-3794.
40. A. Suzuki, Y. Mishin, *J. Mater. Sci.* 40 (2005): p. 3155-3161.
41. P. Keblinski, D. Wolf, S.R. Phillpot, H. Gleiter, *Philos. Mag. A* 79 (1999): p. 2735-2761.
42. P. Keblinski, S.R. Phillpot, D. Wolf, *Phys. Rev. Lett.* 77 (1996): p. 2965-2968.
43. T.E. Hsieh, R.W. Balluffi, *Acta Metall.* 37 (1989): p. 1637-1644.
44. A.M. Alsayed, M.F. Islam, J. Zhang, P.J. Collings, A.G. Yodh, *Science* 309 (2005): p. 1207-1210.
45. D.R. Clarke, *J. Am. Ceram. Soc.* 70 (1987): p. 15-22.
46. D.R. Clarke, T.M. Shaw, A.P. Philipse, R.G. Horn, *J. Am. Ceram. Soc.* 76 (1993): p. 1201-1204.
47. V.K. Gupta, D.H. Yoon, H.M. Meyer III, J. Luo, *Acta Mater.* 55 (2007): p. 3131-3142.
48. J. Luo, V.K. Gupta, D.H. Yoon, H.M. Meyer, *Appl. Phys. Lett.* 87 (2005): p. 231902.
49. J. Huang, J. Luo, *Phys. Chem. Chem. Phys.* 16 (2014): p. 7786-7798.
50. A. Kayyar, H.J. Qian, J. Luo, *Appl. Phys. Lett.* 95 (2009): p. 221905.
51. H.J. Qian, J. Luo, Y.M. Chiang, *Acta Mater.* 56 (2008): p. 862-873.
52. H. Qian, J. Luo, *Acta Mater.* 56 (2008): p. 4702-4714.
53. H.J. Qian, J. Luo, *Appl. Phys. Lett.* 91 (2007): p. 061909.
54. J. Luo, Y.-M. Chiang, R.M. Cannon, *Langmuir* 21 (2005): p. 7358-7365.
55. J. Luo, Y.-M. Chiang, *Acta Mater.* 48 (2000): p. 4501-4515.
56. J. Luo, Y.-M. Chiang, *J. Eur. Ceram. Soc.* 19 (1999): p. 697-701.
57. M. Baram, D. Chatain, W.D. Kaplan, *Science* 332 (2011): p. 206-209.
58. M. Baram, W.D. Kaplan, *J. Mater. Sci.* 41 (2006): p. 7775-7784.
59. H. Wang, Y.-M. Chiang, *J. Am. Ceram. Soc.* 81 (1998): p. 89-96.
60. V.K. Gupta, D.H. Yoon, J. Luo, H.M. Meyer III, "Preliminary Results of Activated Sintering Mechanism and Grain Boundary Prewetting/Premelting in Nickel-Doped Tungsten," in *Ceramic Nanomaterials and Nanotechnology IV*, eds. R.M. Laine, M. Hu, S. Lu, Ceramic Transactions, vol. 172 (Hoboken, NJ: John Wiley & Sons, 2005).
61. I. MacLaren, R.M. Cannon, M.A. Gülgün, R. Voytovych, N.P. Pogrion, C. Scheu, U. Täffner, M. Rühle, *J. Am. Ceram. Soc.* 86 (2003): p. 650.
62. M. Tang, W.C. Carter, R.M. Cannon, *Phys. Rev. Lett.* 97 (2006): p. 075502.
63. Y. Mishin, W.J. Boettinger, J.A. Warren, G.B. McFadden, *Acta Mater.* 57 (2009): p. 3771-3785.
64. B.B. Straumal, O.I. Noskovich, V.N. Semenov, L.S. Shvindlerman, W. Gust, B. Predel, *Acta Metall. Mater.* 40 (1992): p. 795-801.
65. E.I. Rabkin, V.N. Semenov, L.S. Shvindlerman, B.B. Straumal, *Acta Metall. Mater.* 39 (1991): p. 627-639.
66. O.I. Noskovich, E.I. Rabkin, V.N. Semenov, B.B. Straumal, L.S. Shvindlerman, *Acta Metall. Mater.* 39 (1991): p. 3091-3098.
67. X. Shi, J. Luo, *Phys. Rev. B* 84 (2011): p. 014105.
68. X. Shi, J. Luo, *Phys. Rev. Lett.* 105 (2010): p. 236102.
69. E.W. Hart, *Scrip. Metal.* 2 (1968): p. 179-182.
70. E.W. Hart, "Grain Boundary Phase Transformations," in *Nature and Behavior of Grain Boundaries*, ed. H. Hu (New York, NY: Plenum, 1972), p. 155-170.
71. M.P. Seah, *J. Phys. F: Metal Physics* 10 (1980): p. 1043-1064.
72. E.D. Hondros, M.P. Seah, *Metall. Trans. A* 8 (1977): p. 1363-1371.
73. J.W. Cahn, *J. de Physique* 43 (1982): p. C6.
74. R. Kikuchi, J.W. Cahn, *Phys. Rev. B* 21 (1980): p. 1893-1897.
75. R. Kikuchi, J.W. Cahn, *Phys. Rev. B* 36 (1987): p. 418.
76. M. Tang, W.C. Carter, R.M. Cannon, *Phys. Rev. B* 73 (2006): p. 024102.
77. C.M. Bishop, R.M. Cannon, W.C. Carter, *Acta Mater.* 53 (2005): p. 4755-4764.
78. W.D. Kaplan, D. Chatain, P. Wynblatt, W.C. Carter, *J. Mater. Sci.* 48 (2013): p. 5681-5717.
79. P. Wynblatt, D. Chatain, *Mater. Sci. Eng. A* 495 (2008): p. 119-125.
80. P. Wynblatt, D. Chatain, *Metall. Mater. Trans. A* 37 (2006): p. 2595-2620.
81. T. Frolov, Y. Mishin, *J. Chem. Phys.* 143 (2015): p. 044706.
82. T. Frolov, M. Asta, Y. Mishin, *Phys. Rev. B* 92 (2015): p. 020103.
83. T. Frolov, D.L. Olmsted, M. Asta, Y. Mishin, *Nature Communications* 4 (2013): p. 1899.
84. T. Frolov, S.V. Divinski, M. Asta, Y. Mishin, *Phys. Rev. Lett.* 110 (2013): p. 255502.
85. J. Luo, X.M. Shi, *Appl. Phys. Lett.* 92 (2008): p. 101901.
86. J. Luo, *Appl. Phys. Lett.* 95 (2009): p. 071911.
87. J. Luo, *J. Am. Ceram. Soc.* 95 (2012): p. 2358-2371.
88. S. Ma, K. Meshinchi Asl, C. Tansarawiput, P.R. Cantwella, M. Qi, M.P. Harmer, J. Luo, *Scrip. Mater.* 66 (2012): p. 203-206.
89. S. Ma, P.R. Cantwell, T.J. Pennycook, N. Zhou, M.P. Oxley, D.N. Leonard, S.J. Pennycook, J. Luo, M.P. Harmer, *Acta Mater.* 61 (2013): p. 1691-1704.
90. S.J. Dillon, M.P. Harmer, *Acta Mater.* 55 (2007): p. 5247-5254.
91. S.J. Dillon, M. Tang, W.C. Carter, M.P. Harmer, *Acta Mater.* 55 (2007): p. 6208-6218.
92. M.P. Harmer, *J. Am. Ceram. Soc.* 93 (2010): p. 301-317.
93. M.P. Harmer, *Science* 332 (2011): p. 182-183.
94. J. Luo, H. Wang, Y.-M. Chiang, *J. Am. Ceram. Soc.* 82 (1999): p. 916.
95. J. Luo, *Curr. Opin. Solid State Mater. Sci.* 12 (2008): p. 81-88.
96. S.J. Dillon, M.P. Harmer, *J. Eur. Ceram. Soc.* 28 (2008): p. 1485-1493.
97. N. Zhou, J. Luo, *Acta Mater.* 91 (2015): p. 202-216.

98. J.S. Lee, K. Klockgeter, C. Herzig, *Colloque De Physique* 51 (1990): p. C1-569.
99. K. Wolski, V. Laporte, N. Marie, M. Biscondi, *Interf. Sci.* 9 (2001): p. 183-189.
100. N. Marie, K. Wolski, M. Biscondi, *Scrip. Mater.* 43 (2000): p. 943-949.
101. N. Marie, K. Wolski, M. Biscondi, *J. Nucl. Mater.* 296 (2001): p. 282-288.
102. J. Kang, G.C. Glatzmaier, S.H. Wei, *Phys. Rev. Lett.* 111 (2013): p. 055502.
103. Q. Gao, M. Widom, *Phys. Rev. B* 90 (2014): p. 144102.
104. G. Duscher, M.F. Chisholm, U. Alber, M. Ruhle, *Nat. Mater.* 3 (2004): p. 621-626.
105. R. Schweinfest, A.T. Paxton, M.W. Finnis, *Nature* 432 (2004): p. 1008-1011.
106. M. Yamaguchi, M. Shiga, H. Kaburaki, *Science* 307 (2005): p. 393-397.
107. H.P. Chen, R.K. Kalia, E. Kaxiras, G. Lu, A. Nakano, K. Nomura, A.C.T. van Duin, P. Vashishta, Z.S. Yuan, *Phys. Rev. Lett.* 104 (2010): p. 155502.
108. J.R. Rice, J.-S. Wang, *Mater. Sci. Eng. A* 107 (1989): p. 23.
109. J. Zhang, N. Li, *J. Nucl. Mater.* 373 (2008): p. 351-377.
110. J. Zhang, N. Li, *Corrosion* 60 (2004): p. 331-341.
111. J. Zhang, N. Li, *Oxid. Met.* 63 (2005): p. 353-381.
112. J. Zhang, T.F. Marcille, R. Kapernick, *Corrosion* 64 (2008): p. 563-573.
113. J. Zhang, *Corros. Sci.* 51 (2009): p. 1207-1227.
114. W.W. Mullins, *J. Appl. Phys.* 28 (1957): p. 333-339.
115. W.W. Mullins, *Trans. Metal Soc. AIME* 218 (1960): p. 354-361.
116. E.E. Glickman, *Metall. Mater. Trans. A* 42 (2011): p. 250-266.
117. M. Schick, "An Introduction to Wetting Phenomena," in *Les Houches Summer School Lectures, Session XLVIII*, eds. J. Charvolin, J.F. Joanny, J. Zinn-Justin (Amsterdam, The Netherlands: Elsevier, 1990), p. 415-497.
118. S. Dietrich, Wetting Phenomena, " in *Phase Transitions and Critical Phenomena*, eds. C. Domb, J.L. Lebowitz, vol. 12 (London, United Kingdom: Academic Press, 1988), p. 1-218.
119. P.G. de Gennes, *Reviews of Modern Physics* 57 (1985): p. 827-863.